Implicating SCF Complexes in Organogenesis in *Caenorhabditis elegans*

Stanley R. G. Polley,[1] Aleksandra Kuzmanov,[1] Jujiao Kuang,[1] Jonathan Karpel,[1] Vladimir Lažetić, Evguenia I. Karina, Bethany L. Veo, and David S. Fay[2]

Department of Molecular Biology, College of Agriculture and Natural Resources, University of Wyoming, Laramie, Wyoming 82071

ABSTRACT Development of the *Caenorhabditis elegans* foregut (pharynx) is regulated by a network of proteins that includes the Retinoblastoma protein (pRb) ortholog LIN-35; the ubiquitin pathway components UBC-18 and ARI-1; and PHA-1, a cytoplasmic protein. Loss of *pha-1* activity impairs pharyngeal development and body morphogenesis, leading to embryonic arrest. We have used a genetic suppressor approach to dissect this complex pathway. The lethality of *pha-1* mutants is suppressed by loss-of-function mutations in *sup-35*/*ztf-21* and *sup-37*/*ztf-12*, which encode Zn-finger proteins, and by mutations in *sup-36*. Here we show that *sup-36* encodes a divergent Skp1 family member that binds to several F-box proteins and the microtubule-associated protein PLT-1/τ. Like SUP-35, SUP-36 levels were negatively regulated by UBC-18–ARI-1. We also found that SUP-35 and SUP-37 physically associated and that SUP-35 could bind microtubules. Thus, SUP-35, SUP-36, and SUP-37 may function within a pathway or complex that includes cytoskeletal components. Additionally, SUP-36 may regulate the subcellular localization of SUP-35 during embryogenesis. We carried out a genome-wide RNAi screen to identify additional regulators of this network and identified 39 genes, most of which are associated with transcriptional regulation. Twenty-three of these genes acted via the LIN-35 pathway. In addition, several S-phase kinase-associated protein (Skp)1–Cullin–F-Box (SCF) components were identified, further implicating SCF complexes as part of the greater network controlling pharyngeal development.

THE analysis of suppressor and enhancer mutations is an invaluable tool for elucidating the molecular pathways and networks that control animal development. Using this approach, we have identified a multigene module that controls organogenesis of the *Caenorhabditis elegans* pharynx (foregut). This network includes the *C. elegans* Retinoblastoma family ortholog, LIN-35/pRb, and a conserved E2–E3 ubiquitin modification complex, UBC-18/UBCH7–ARI-1/AR1H1 (Fay *et al.* 2003; Qiu and Fay 2006). LIN-35 and UBC-18–ARI-1 negatively regulate a Zn-finger protein, SUP-35/ZTF-21, at the level of transcription and protein stability, respectively (Mani and Fay 2009). Furthermore, SUP-35, along with a second Zn-finger protein, SUP-37/ZTF-12, functionally opposes PHA-1, a novel cytoplasmic protein that is required for *C. elegans* embryonic development (Schnabel and Schnabel 1990; Granato *et al.* 1994; Fay *et al.* 2004, 2012). Our working model is that in the absence of both *lin-35* and *ubc-18* activities, SUP-35 levels are abnormally elevated, which in turn interferes with the ability of PHA-1 to carry out essential functions during embryogenesis.

Loss-of-function (LOF) mutations in *pha-1* lead to gross defects in pharyngeal development and body morphology (Schnabel and Schnabel 1990; Fay *et al.* 2004, 2012). Specifically, PHA-1 plays a role in both establishing and maintaining a stable attachment between the anterior epithelial cells of the developing pharynx and the arcade cells that compose the future buccal cavity (mouth) (Fay *et al.* 2004). This is in part due to the failure of anterior pharyngeal epithelial cells to undergo stereotypical changes in shape and apical–basal polarity, a step that has been termed reorientation (Portereiko and Mango 2001; Fay *et al.* 2004). When reorientation fails, a connection between the pharynx and arcade cells does not form, which precludes the generation of an intact intestinal tract (Portereiko *et al.* 2004). The result is a highly penetrant **p**harynx **un**attached (Pun) phenotype, whereby animals are unable to feed and therefore arrest as L1 larvae. In addition, strong LOF mutations in *pha-1* lead to gross defects in body morphogenesis, which prevent animals

doi: 10.1534/genetics.113.158485
Manuscript received October 9, 2013; accepted for publication October 29, 2013; published Early Online November 5, 2013.
Supporting information is available online at http://www.genetics.org/lookup/suppl/doi:10.1534/genetics.113.158485/-/DC1.
[1]These authors contributed equally to this work.
[2]Corresponding author: Department 3944, 1000 E. University Ave., Department of Molecular Biology, College of Agriculture and Natural Resources, University of Wyoming, Laramie, WY 82071. E-mail: davidfay@uwyo.edu

from completing embryogenesis and hatching. Similar phenotypes are also observed in *lin-35*; *ubc-18* mutants, as well as in other related compound mutants, and in strains that overexpress SUP-35 (Fay *et al.* 2003; Mani and Fay 2009).

Notably, LOF mutations in *sup-35* and *sup-37* completely suppress the lethality of *pha-1* LOF mutants, including several molecular nulls (Schnabel *et al.* 1991; Mani and Fay 2009; Fay *et al.* 2012). This observation, together with other data, has led to the hypothesis that SUP-35 and SUP-37 act in a pathway or complex that is in opposition to PHA-1, possibly through the regulation of a mutual downstream target or biological processes. In addition, LOF mutations in *sup-35* and *sup-37* suppress the synthetic lethality of *lin-35*; *ubc-18*, *lin-35*; *pha-1*, and *ari-1*; *pha-1* double mutants (Fay *et al.* 2004, 2012; Qiu and Fay 2006; Mani and Fay 2009). Here we describe the molecular characterization of *sup-36*, a gene in which mutations are capable of suppressing the lethality of *pha-1* and *lin-35*; *ubc-18* mutants. *sup-36* encodes a Skp1-related protein that binds to several F-box proteins and to the microtubule-associated protein PTL-1/τ. In addition, by carrying out a genome-wide RNAi screen for suppressors of *lin-35*; *ubc-18* larval lethality, we have identified 37 additional genes whose functions intersect with this regulatory network.

Materials and Methods

Strains and maintenance

C. elegans strains were maintained according to standard methods (Stiernagle 2005). Strains used in this study include GE24 [*pha-1(e2123) III*], WY83 [*lin-35(n745) I*; *ubc-18(ku254) III*; *kuEx119* (*lin-35*+; *sur-5*::*GFP*)], WY119 [*lin-35(n745) I*; *pha-1(fd1) III*; *kuEx119*], WY163 [*pha-1(e2123) III*; *sup-36(e2217) IV*], GE341 [*pha-1(e2123) dpy-18(e499) III*; *sup-36(e2217) IV*], GE342 [*pha-1(e2123) dpy-18(e499) III*; *sup-36(e2218) IV*], GE391 [*pha-1(e2123) dpy-18(e499) III*; *sup-37(t1012) IV*], GE397 [*pha-1(e2123) dpy-18(e499) III*; *sup-36(t1956) IV*], GE398 [*pha-1(e2123ts) dpy-18(e499) III*; *sup-36(t1957) IV*], WY160 [*pha-1(e2123)* backcrossed five times to CB4856], WY158 [*pha-1(e2123) III*; *dpy-13(e184) unc-24(e138) IV*], WY805 [*pha-1(e2123) III*; *sup-36(e2217) IV*; *fdEx201*], WY512 [*sup-36(t1956) IV*; *fdEx57(rol-6(gf)* + *SUP-35*::*GFP)*], WY865 [*ari-1(tm2549) I*; *pha-1(e2123) III*; *fdEx201(pha-1*+; *sur-5*::*RFP)*], WY729 [*pha-1(e2123) III*; *fdEx121(wild-type sup-36* + *surp-5*::*GFP)*], WY730 [*pha-1(e2123) dpy-18(e499)*; *fdEx121(sup-36 genomic locus* + *sur-5*::*GFP)*], WY862 [*sup-35(tm1810) III*; *sup-36(e2217) IV*; *sup-37(e2215) V*; *Ex*($P_{pha\text{-}1}$::*GFP*)], WY925 [*fdEx115(rol-6(gf)*; *SUP-36*::*GFP*)], WY999 [*fdEx57*], and WY1000 [*sup-35(tm1810) III*; *sup-36(e2217) IV*; *sup-37(e2215) V*; *fdEx238(rol-6(gf)*; *SUP-36*::*GFP*)]. Deletion alleles for *sup-36* (*tm3912*), *pha-1* (*tm3569* and *tm3671*), and *ari-1* (*tm2549*) were obtained from the National BioResource Project (NBRP) Tokyo, Japan.

Genetic mapping and molecular identification of sup-36

Preliminary mapping placed *sup-36* on LGIV (data not shown) (Schnabel *et al.* 1991). To narrow the *sup-36* genomic region, three-point mapping was performed using the balanced strain *pha-1(e2123) III*; *dpy-13(e184) unc-24(e138)/sup-36(e2217) IV*. Of the progeny, 6/53 Dpy non-Unc and 82/87 Unc non-Dpy animals acquired the *sup-36* mutation. For single-nucleotide polymorphism (SNP) mapping, *pha-1(e2123)* hermaphrodites were backcrossed five times to CB4856 Hawaiian males, and the resulting *pha-1(e2123)*; CG4856–5× males (WY160) were crossed to *pha-1(e2123)*; *dpy-13 sup-36(e2217) unc-24* hermaphrodites, followed by standard SNP mapping procedures (Fay 2006). After an analysis of ∼500 Dpy non-Unc and Unc non-Dpy recombinants, the *sup-36* mutation was isolated to an ∼80-kb region containing 38 genes between SNPs located on cosmids C01G5 and C01B10. Rescue experiments were performed by amplifying a 1984-bp PCR fragment (chromosome IV, 6,600,477–6,602,461) encompassing the *sup-36* genomic region from wild-type animals, using primers 5′-GAAGAGTCTAATTAAGAGTACTGCCGA-3′ and 5′-AG ATTTGTGAGCACATTTCGAGA-3′.

Sequence alignments

Alignments were carried out using MAFFT (http://www.ebi.ac.uk/Tools/msa/mafft/) and MUSCLE (http://www.ebi.ac.uk/Tools/msa/muscle/). After the alignments were reformatted in Phylip4 (http://www.ebi.ac.uk/cgi-bin/readseq.cgi), model testing was carried out (http://darwin.uvigo.es/software/prottest2_server.html), and optimal models were used to generate trees (http://www.atgc-montpellier.fr/phyml/). Both MAFFT and MUSCLE alignment programs produced nearly identical dendrograms (data not shown).

Microscopy

Quantitative fluorescence microscopy was performed using a Nikon Eclipse microscope. Quantification of GFP fluorescence in embryos was carried out using Open Lab Software Version 5.0.2. All images were captured using identical exposure times, and all embryos used in our analysis were of similar developmental stages (∼200–300 cells). Averages of the mean fluorescence were calculated to compare expression levels. *P*-values were determined using a two-tailed Student's *t*-test. Confocal images were acquired using a 100× (1.4 NA) or a 60× (1.49 NA) objective on an Olympus IX-71 inverted microscope. The microscope was equipped with a CSU-X1 spinning disc head (Yokogawa) and a cooled EMCCD camera (ImagEM, Hamamatsu). Image acquisition and microscope automation were controlled using Metamorph software (Molecular Devices).

Yeast two-hybrid analysis

Physical interactions between SUP-36 and FBXC-53, FBXC-32, FBXC-20, and PTL-1 were tested by yeast two-hybrid (Y2H) analysis, using the ProQuest Two-Hybrid System (Invitrogen, Carlsbad, CA). Bait and prey plasmids were generated using the Gateway cloning system. Gateway entry clones for *fbxc-53*, *fbxc-32*, and *fbxc-20* were a generous gift from Michael Calderwood and Mark Vidal, Harvard Medical

School, Boston, MA (Li *et al.* 2004; Simonis *et al.* 2009). To generate a Gateway entry clone for *ptl-1*, a *ptl-1a* cDNA was PCR amplified using the following primers: 5′-GGGGACAAGTTTG TACAAAAAAGCAGGCTCCATGTCAACCCCTCAATCAG-3′ and 5′-GGGGACCACTTTGTACAAGAAAGCTGGGTTTCATAACG AGCTGATGTC-3′. The resulting amplicon was cloned into the donor vector pDONR221. Genes in the entry clones were transferred to the yeast expression vectors in a Gateway LR recombination reaction with the bait destination vector pDEST32 (*sup-36*) or the prey destination vector pDEST22 (*fbxc-53*, *fbxc-32*, *fbxc-20*, and *ptl-1a*). All plasmids were sequenced and tested for self-activation of the reporter *HIS3* by growth on histidine-minus (histidine-dropout) medium in the presence of varying levels of 3-amino-1,2,4-triazole (3-AT). Yeast strain MaV203 was cotransformed with the *sup-36* bait vector (or the control empty bait vector) and each of the prey vectors (or the control empty prey vector). Transformants were patched onto a SC-Leu-Trp master plate along with the negative activation controls (bait with empty prey vector and preys with empty bait vector) and positive and negative interaction controls supplied by Invitrogen. After 18 hr of incubation at 30°, patches were replica plated to SC-Leu-Trp-Ura and SC-Leu-Trp-His + 25 mM 3-AT plates, and the latter were immediately replica cleaned. Plates were then incubated at 30° for 24 hr, replica cleaned, and incubated for 48 hr at 30°. To test for inhibition of growth on 5-fluoroorotic acid (5-FOA) plates, candidate yeast colonies were streaked onto 0.2% 5-FOA selection plates and the extent of colony growth was determined after 72 hr. The quantitative assay for β-galactosidase (β-gal) activity was performed following the manufacturer's instructions in liquid cultures, using chlorophenol red-β-D-galactopyranoside (CPRG) as a substrate. β-gal levels were calculated using the following equation: β-gal = (1000 × absorbance at 574 nm)/[(duration of reaction) × (sample volume) × (absorbance at 600 nm)]. Controls supplied by Invitrogen were as follows: strong positive interaction, Krev1/RalGDS-wt; weak positive interaction, Krev1/RalGDS-m1; and negative interaction control, Krev1/RalGDS-m2.

SUP-36 reporter plasmid construction

A SUP-36::GFP translation fusion reporter was generated by amplifying coding sequences along with the 5′-regulatory region of *sup-36* from N2 genomic DNA, using primers 5′-CTGCCGAGTTTGAATAAAGAT-3′ and 5′-CATGAGTCTAGATAG TGCAAGTTCTGAAATGAT-3′. The DNA fragment was digested with *Hin*dIII and *Xba*I and was then cloned into corresponding sites in pPD95.75 (Addgene). Sequence analysis was used to confirm the absence of mutations. A $P_{sup\text{-}36}$::GFP transcriptional fusion reporter was generated by amplifying with primers 5′-CTGCCGAGTTTGAATAAAGAT-3′ and 5′-CATGAGTCTAGAT AGTGCAAGTTCTGAAATGAT-3′, digesting with *Hin*dIII and *Xba*I, and cloning into the corresponding sites in pPD95.75.

RNA interference

RNA interference (RNAi) was carried out using strains from the Geneservice Library, following standard feeding protocols (Ahringer 2005). Whole-genome RNAi suppressor screening was carried out as described in Polley and Fay (2012). All positive RNAi clones were confirmed by carrying out at least three independent repeats, and clones were sequenced to verify their molecular identities (Supporting Information, Table S1). Double-stranded (ds)RNA for *sup-36(RNAi)* injection was prepared using RiboMAX Large Scale RNA Production Systems (T7), using primers 5′-TAA TACGACTCACTATAGGGGCCATCTTGCGAGATCAAAT-3′ and 5′-TAATACGACTCACTATAGGGCCTTAAAATCAATTTGAAAA AGTTCTG-3′. dsRNA was injected into young adults at ∼1.0 μg/μl, and F_1 progeny were scored for viability.

Immunoprecipitation assays

A full-length complementary (c)DNA of SUP-35 was cloned into the *Bam*HI and *Xho*I sites of pET-26b(+) (Novagen) to create an in-frame fusion with the 6× His tag, using the primer set 5′-ATTAAGGATCCGTGGCTCACACTTTTGCGTGCC-3′ and 5′-ACACGGCTCGAGAATTGAGCACAAGTCAAGGG-3′. His-tagged SUP-35 was expressed in Rosetta (DE3; EMD Biosciences); expression was induced with 0.5 mM isopropyl 1-thio-β-D-galactopyranoside (IPTG) at 37° for 4 hr.

Two primers (5′-GGATCCTAATACGACTCACTATAGG GAACAGCCACCATGCCATCTTGCGAGATCAAATTC-3′ and 5′-CTATTGGACATTCTGGAAAGCGTCTGCT-3′) were used to amplify a full-length *sup-36* cDNA containing an upstream bacteriophage T7 promoter and a Kozak consensus sequence, using Pfu DNA polymerase (Thermo Scientific). Likewise, a second set of primers (5′-GGATCCTAATAC GACTCACTATAGGGAACAGCCACCATGAGCATCAGCGGAGA GGACAAC-3′ and 5′-TTAATCAGAAGAGACACCATCATCAT CTTCTTCCATC-3′) was used to amplify *sup-37*. Both PCR products were sequenced and used to generate radiolabeled protein *in vitro* with [^{35}S]methionine, using the TNT T7 Quick for PCR DNA system (Promega, Madison, WI). Expression of correctly sized ^{35}S-labeled proteins was confirmed by SDS–PAGE and autoradiography. Binding assays were performed using the Pierce His Protein Interaction Pull-Down Kit (Thermo Scientific). Eluted proteins were analyzed by SDS–PAGE (7% acrylamide) and detected by autoradiography (SUP-36 and SUP-37) and Coomassie staining (SUP-35).

Microtubule binding assays

pET-26b–SUP-35 was constructed and expressed as described above. His-tagged SUP-35 was purified using the Pierce His Protein Interaction Pull-Down Kit. To increase its solubility, purified protein was dialyzed against Tris buffer (pH 8.0) and then was centrifuged at 100,000 × *g* for 40 min, using a Beckman (Fullerton, CA) TL-100 ultracentrifuge. The supernatant was saved for the microtubule-binding assay. Microtubule-binding assays were performed using the Microtubule Binding Protein Spin-Down Assay Biochem Kit (Cytoskeleton). SUP-35 binding was analyzed by SDS–PAGE (7% acrylamide) and detected with SYPRO Ruby Protein Gel Stain (Molecular Probes, Eugene, OR). Negative and positive controls for microtubule binding were

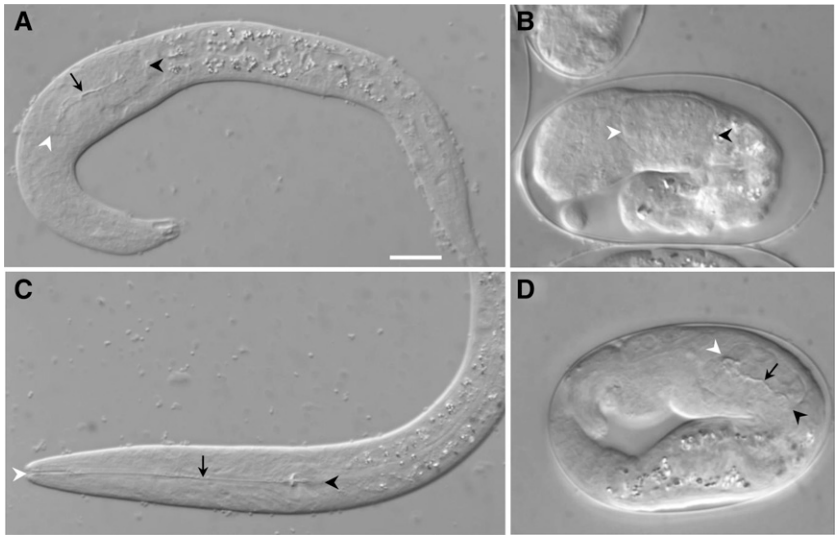

Figure 1 Pharyngeal phenotypes of *pha-1* mutants and suppressed strains. (A–D) DIC micrographs of L1-stage larvae (A and C) and embryos (B and D) are shown. A and B show *pha-1(ts)* mutants grown at the nonpermissive temperatures of 22° and 25°, respectively. Note abnormal, compressed pharyngeal structures at both temperatures, whereas body morphogenesis defects are more severe at the higher temperature. C shows a suppressed *pha-1(ts); sup-36 (e2217)* double mutant grown at 25° with a normal pharynx and body morphology. D shows a *pha-1* embryo grown at the permissive temperature of 16° with overexpression of *sup-36* by an extrachromosomal array (*fdEx121*). Open and solid arrowheads indicate anterior and posterior boundaries of the pharynx, respectively. Solid arrows delineate the pharyngeal lumen. Bar in A, 10 μm for A–D.

analyzed by SDS–PAGE (7% acrylamide) and detected by Coomassie staining.

Results

sup-36 encodes a divergent member of the Skp1 family of proteins

LOF mutations in the *C. elegans* gene *pha-1* lead to a fully penetrant embryonic and larval arrest and display gross defects in pharyngeal development and body morphogenesis (Figure 1, A and B) (Schnabel and Schnabel 1990). Recessive mutations in the *sup-36* locus were identified in a genetic screen for suppressors of *pha-1* LOF lethality (Schnabel *et al.* 1991). *sup-36* mutations suppressed two temperature-sensitive alleles of *pha-1*, including *pha-1(e2123)* [*pha-1 (ts)*] (Figure 1C). We mapped *sup-36* to a region on chromosome IV that contains 38 genes, using conventional genetic and SNP-mapping methods. Sequence analysis of several candidate genes identified a region that was deleted in strains carrying the canonical allele of *sup-36*, *e2217*. We determined that the *e2217* deletion encompasses six contiguous genes (*nspb-3*, F38A5.6, *nspb-4*, *nspb-5*, F38A5.8, and F38A5.7). Although the precise endpoints of the *e2217* deletion were not determined, F38A5.11/*irld-7* and F15B10.3, which bracket the six deleted genes, were not affected by *e2217*, and thus the total size of the *e2217* deletion is likely to be <7 kb.

Further analysis of the six genes within the deleted region specifically implicated F38A5.7 as *sup-36*. First, expression of wild-type copies of F38A5.7 from an extrachromosomal array completely reverted the viability of *pha-1 (ts)*; *sup-36(e2217)* double mutants at 25° in three of three independent lines tested. Moreover, *pha-1(ts)*; *sup-36 (e2217)* animals that contained the F38A5.7 array (marked by *sur-5*::GFP) arrested as embryos with a Pun phenotype that was identical to that of *pha-1(ts)* single mutants at 25° (data not shown). Second, dsRNA injection of F38A5.7 [*sup-36(RNAi)*] suppressed *pha-1(ts)* lethality at 25° (Table 1). Third, sequencing of additional alleles of *sup-36* identified multiple independent mutations within F38A5.7 (see below), whereas mutations in other genes within the *e2217*-deleted region were not detected (data not shown). We therefore designated F38A5.7 as *sup-36*.

sup-36 contains two exons and encodes a predicted protein of 169 amino acids (Figure 2). Sequence analysis identified a single paralog of *sup-36* in *C. elegans*, F15B10.3, which resides immediately downstream of *sup-36* on LGIV and is the result of an apparent gene duplication event within the *C. elegans* lineage. SUP-36 is 65% identical and 83% similar to F15B10.3, but, unlike SUP-36, F15B10.3 is encoded by three exons (Figure 2B and data not shown). Sequence homology searches also identified a number of SUP-36–like proteins in related nematode species as well as several proteins with homology to SUP-36 in nonnematode organisms (Figure 2B and data not shown). Interestingly, two of the genes from nonnematode species are annotated members of the conserved family of S-phase kinase-associated proteins (Skp). Skp1 proteins form multisubunit E3 (ubiquitin ligase) complexes with F-box proteins and cullins [Skp1–Cullin–F-Box (SCF) complexes] and target a wide range of proteins for degradation by the proteasome (Deshaies 1999; Willems *et al.* 2004; Kipreos 2005). SUP-36 is 21% identical and 40% similar to the microsporidia Skp1-like protein AFN82639 and 18% identical and 44% similar to XP_002513359 from castor bean (Figure 2B). In addition, SUP-36 is 18% identical and 39% similar to human Skp1, whereas AFN82639 and XP_002513359 are both 33% identical to human Skp1 (Figure 2B). Consistent with these observations, Pfam analysis identified Skp1 dimerization domains spanning amino acid residues 100–145 of SUP-36 ($P = 0.00088$) and 121–167 of F15B10.3 ($P = 0.0066$; Figure 2B). Phylogenetic analysis further suggested that SUP-36 and F15B10.3 are indeed divergent members of the Skp1 family of proteins (Figure S1).

A hallmark of Skp1 family members is their association with F-box proteins (Deshaies 1999; Kipreos and Pagano 2000; Willems *et al.* 2004). Notably, SUP-36 exhibits high-

Table 1 Suppression of pharyngeal defects by *sup-36*

Genotype (temperature)	Fertile adults (%)
pha-1(e2123ts) (16°)	91 (*n* = 285)
pha-1(e2123ts) (25°)	0 (*n* = 310)
pha-1(e2123); sup-36(e2217) (25°)	95 (*n* = 320)
pha-1(e2123); sup-36(RNAi) (25°)	97 (*n* = 438)
pha-1(tm3671) (20°)	0 (*n* = 252)
pha-1(tm3671); sup-36(e2217) (20°)	76 (*n* = 695)
pha-1(tm3569) (20°)	0 (*n* = 279)
pha-1(tm3569); sup-36(e2217) (20°)	81 (*n* = 349)
lin-35(n745); pha-1(fd1) (20°)	0 (*n* = 248)
lin-35(n745); pha-1(fd1); sup-36(RNAi) (20°)	75 (*n* = 276)
lin-35(n745); ubc-18(ku254) (20°)	0 (*n* = 137)
lin-35(n745); ubc-18(ku254); sup-36(e2217) (20°)	70 (*n* = 118)
ari-1(tm2549); pha-1(e2123) (16°)	0 (*n* = 255)
ari-1(tm2549); pha-1(e2123); sup-36(RNAi) (16°)	90 (*n* = 811)

confidence (termed "core") physical interactions with three *C. elegans* F-box proteins (FBXC-20, FBXC-32, and FBXC-53), based on Y2H analyses (Li *et al.* 2004; Simonis *et al.* 2009). Furthermore, SUP-36 binds to FBXC-20 in *in vitro* immunoprecipitation assays (Simonis *et al.* 2009). Using independently generated Y2H clones and strains, we found that SUP-36 indeed showed physical interactions with FBXC-20 and FBXC-53 (Figure 3 and Figure S2). Among the three F-box proteins, interactions between SUP-36 and FBXC-53 were the strongest, leading to positive outcomes in His−, Ura−, 5-FOA, and β-gal assays (Figure 3 and Figure S2). Interactions between SUP-36 and FBXC-20 were weaker but nevertheless were scored as positive in two of the four standard Y2H assays. These findings further implicate SUP-36 as a divergent member of the Skp1 family of proteins and suggest a possible role for SUP-36 in ubiquitin-mediated proteolysis.

Sequence analysis of three additional alleles of *sup-36* (*e2218*, *e2219*, and *t1956*) identified mutations that lead to nonconservative substitutions at positions G156(R), G121(R), and G63(R), respectively (Figure 2, A and B). All three glycine residues are conserved between SUP-36 and F15B10.3, whereas human Skp1 and XP_002513359 contain alanine residues at the equivalent positions of G63 and G156 of SUP-36 (Figure 2B). The substitution G121R lies within the predicted Skp1 dimerization domain, where equivalent residues from other species are noncharged (Figure 2B). A fourth allele, *t1957*, contains a mutation (G to A) in the first nucleotide of the single *sup-36* intron and is predicted to abolish splicing (Figure 2A) (Blumenthal and Steward 1997). Because the 60-nucleotide intron contains no stop codons and the frame is preserved, this mutation is predicted to result in an insertion of 20 novel amino acids between positions 38 and 39 of the SUP-36 peptide. A fifth allele of *sup-36*, *t1012*, contains a deletion of the entire *sup-36* coding region as well as neighboring sequences, similar

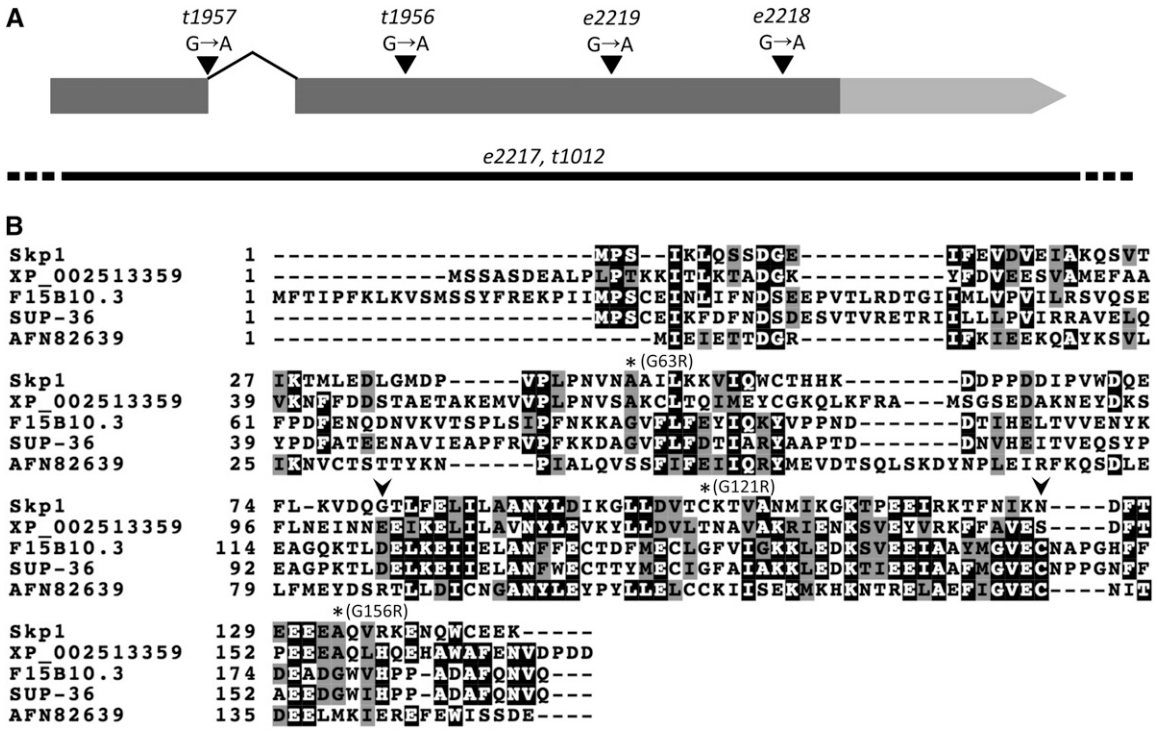

Figure 2 *sup-36* genomic locus and SUP-36 protein sequence. (A) Schematic representation of the *sup-36* genomic locus. Coding regions are indicated by regions with dark shading, and the 3′-UTR is shown as a region with light shading. Six sequenced *sup-36* alleles are shown. *e2217* and *t1012* are deletion alleles (solid line) with endpoints that are not precisely defined (dashed lines). (B) Clustal alignment of SUP-36 and F15B10.3 from *C. elegans*, Skp1 from human, and two Skp1-like proteins from *Encephalitozoon romaleae* (microsporidia; AFN82639) and *Ricinus communis* (castor bean; XP_002513359). Solid blocks with open letters indicate identical amino acid residues; shaded blocks with solid letters indicate similar residues. Three missense mutations are indicated by asterisks. Arrowheads indicate boundaries of the conserved Skp1 dimerization domain.

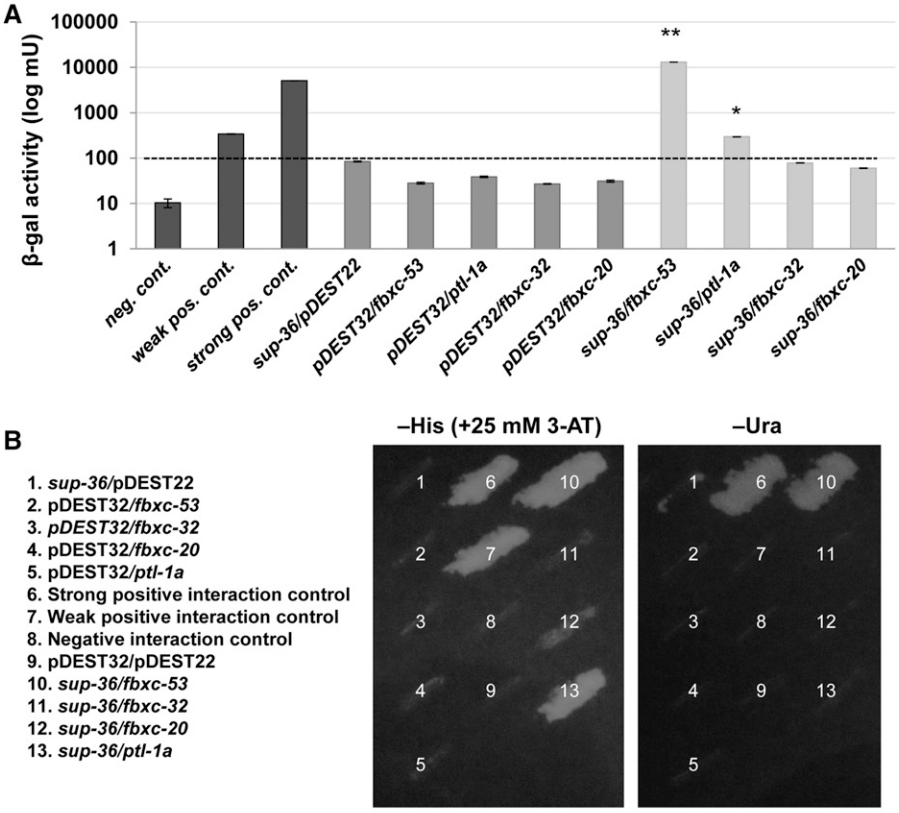

Figure 3 SUP-36 Y2H interactions. (A) Results from a quantitative β-gal assay. Assays were carried out in triplicate, and error bars indicate 95% confidence intervals. Dashed line indicates the value of the highest negative control (*sup-36*/pDEST22). *P*-values were obtained using a Student's *t*-test by comparing the indicated yeast strain to the control *sup-36*/pDEST22 (**$P < 0.01$, *$P < 0.05$). (B) Growth of the indicated yeast strains on His− (+25 mM 3-AT) and Ura− plates. C summarizes results for the four Y2H reporters. +++, strong reporter activation; +, weak interaction; and –, no interaction.

C

Protein pair	–His	–Ura	0.2% 5-FOA	*lacZ*
sup-36/fbxc-53	+++	+++	+++	+++
sup-36/ptl-1a	+++	–	+	+
sup-36/fbxc-32	–	–	–	–
sup-36/fbxc-20	+	–	+	–

to *e2217* (Figure 2A). The identification of mutations affecting the open reading frame of F38A5.7 in all six *sup-36* alleles strongly supports the conclusion that *sup-36* is encoded by F38A5.7. We also note that a strain containing a consortium-generated *sup-36* deletion allele, *tm3912*, is strongly impaired for growth and that this phenotype was not rescued by expression of wild-type *sup-36* from an extrachromosomal array (data not shown). This finding, along with our observation that the *sup-36* deletion mutants *e2217* and *t1012* are not obviously growth impaired, indicates that a closely linked mutation is likely to be responsible for the *tm3912* slow-growth phenotype.

Genetic analysis of sup-36 suppression

LOF mutations in *sup-36* can suppress the embryonic and larval-lethal phenotype of *pha-1(ts)* mutants at 25° (Schnabel *et al.* 1991). We have confirmed these findings along with our previous observations that *sup-36* LOF can suppress the synthetic lethal phenotypes of *lin-35(n745)*; *ubc-18(ku354)* and *lin-35(n745)*; *pha-1(fd1)* double mutants (Table 1) (Fay *et al.* 2004). In addition, the synthetic lethality of *ari-1 (tm2549)*; *pha-1(ts)* mutants at 16° was also suppressed by *sup-36(RNAi)* (Table 1). These findings are consistent with genetic suppression data previously obtained for *sup-35* and *sup-37* and further link these three suppressors to a common cellular function (Qiu and Fay 2006; Mani and Fay 2009; Fay *et al.* 2012). Furthermore, we find that similar to LOF mutations in *sup-35* and *sup-37* (Fay *et al.* 2012), loss of *sup-36* suppressed two null deletion alleles of *pha-1* (*tm3671* and *tm3569*) (Table 1). These latter findings support a model whereby SUP-35/-36/-37 act in parallel to PHA-1 but in a manner that is functionally antagonistic.

During the course of conducting transgenic rescue experiments with wild-type *sup-36*, we noted that overexpression of SUP-36 via extrachromosomal arrays caused lethality in *pha-1(ts)* mutants at 16° but showed no deleterious effect

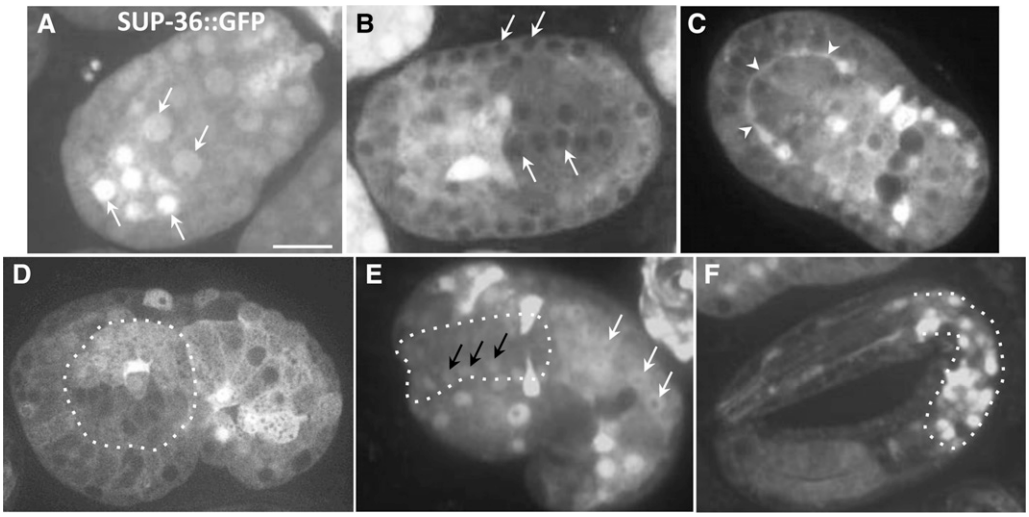

Figure 4 Embryonic expression pattern of SUP-36::GFP. (A–F) Confocal fluorescence images of full-length functional SUP-36::GFP in embryos. A and B show embryos prior to morphogenesis (~100–350 min postfertilization), C and D show embryos at early stages of morphogenesis (~350–400 min), E shows an embryo at the 1.5-fold stage (~430 min), and F shows an ~3-fold-stage embryo (>600 min). Arrows in A, B, and E indicate the positions of nuclei. Arrowheads in C indicate expression of SUP-36::GFP along the basal surface of primordial pharyngeal cells in the region abutting the basement membrane. Dotted outlined regions indicate the developing pharynx. Bar in A, 10 μm for A–F.

on wild type (Figure 1D and data not shown). *pha-1(ts)* mutants that overexpressed *sup-36* arrested as either embryos or L1 larvae and displayed pharyngeal morphogenesis defects typical of *pha-1(ts)* mutants at nonpermissive temperatures. Because the gene product encoded by *pha-1(ts)* has a partially impaired function at the permissive temperature of 16° (Fay *et al.* 2004), it seems likely that reduction of PHA-1 activity rendered the animals more sensitive to toxic effects caused by the overexpression of a protein that normally inhibits or otherwise counteracts PHA-1 downstream functions. Moreover, the toxic effects of SUP-36 overexpression were very similar to those previously observed for overexpression of SUP-35 (Mani and Fay 2009). Notably, LOF of either *sup-35* or *sup-37* suppressed the lethality of *sup-36* overexpression from an extrachromosomal array in the *pha-1(ts)* background (Figure S3), suggesting that *sup-35* and *sup-37* function genetically downstream of *sup-36*. We previously observed, however, that both *sup-36* and *sup-37* can suppress the toxic effects of SUP-35 overexpression (Mani and Fay 2009). A plausible explanation for these conflicting genetic findings is that SUP-35/-36/-37 act at a single common step.

SUP-36 is expressed in a dynamic pattern during embryogenesis

To determine the pattern of *sup-36* expression during development, we generated a construct that encodes the full-length SUP-36 protein fused to GFP at its C terminus. The construct also contains ~1200 bp of sequences upstream of the *sup-36* initiator codon. Importantly, five of five independent extrachromosomal arrays expressing SUP-36::GFP led to lethality of *pha-1(ts)*; *sup-36(e2217)* embryos at 25°, indicating that the SUP-36::GFP fusion protein is functional (Figure S4). In addition, we note that a transcriptional reporter construct ($P_{sup\text{-}36}$::GFP), containing *sup-36* upstream sequences only, showed a similar pattern of expression (data not shown).

SUP-36::GFP was first detected at approximately the 50-cell stage (~100 min postfertilization), at which point it was broadly expressed and localized primarily within nuclei (Figure 4A). Nuclear localization persisted until cells reached the ~200-cell stage (~200 min), at which time SUP-36::GFP was observed predominantly in the cytoplasm (Figure 4B). Beginning in early morphogenesis (~350 min), a ring of SUP-36::GFP expression was often detected in the region abutting the basement membrane that circumscribes the anterior pharyngeal primordium (Figure 4C). As embryonic morphogenesis initiated, localization of SUP-36::GFP became more nuclear and by later stages was enriched in pharyngeal nuclei, particularly within the posterior bulb (Figure 4, D–F). Although the functional significance of the dynamic expression pattern of SUP-36 is currently unclear, the presence of SUP-36 in pharyngeal cells throughout embryogenesis is consistent with an autonomous function in this tissue.

Regulation of SUP-36 by upstream factors

sup-35 is regulated at the level of transcription by LIN-35 and HCF-1 (Mani and Fay 2009; Fay *et al.* 2012). Specifically, LIN-35 functions as a negative regulator of *sup-35* expression, whereas HCF-1 promotes *sup-35* transcription. In addition, SUP-35 is negatively regulated by UBC-18 and ARI-1, which form a conserved E2–E3 complex (Qiu and Fay 2006; Mani and Fay 2009). In contrast, *sup-37* expression is not regulated by LIN-35, HCF-1, or UBC-18–ARI-1 (Fay *et al.* 2012). We found that whereas *sup-36* expression was not regulated by LIN-35 or HCF-1, SUP-36 levels were negatively regulated by UBC-18–ARI-1 (Figure 5). SUP-36::GFP was upregulated ~1.6-fold following RNAi of *ubc-18* or *ari-1*, which is slightly less than the ~2-fold increase previously observed for SUP-35::GFP under these conditions (Fay *et al.*

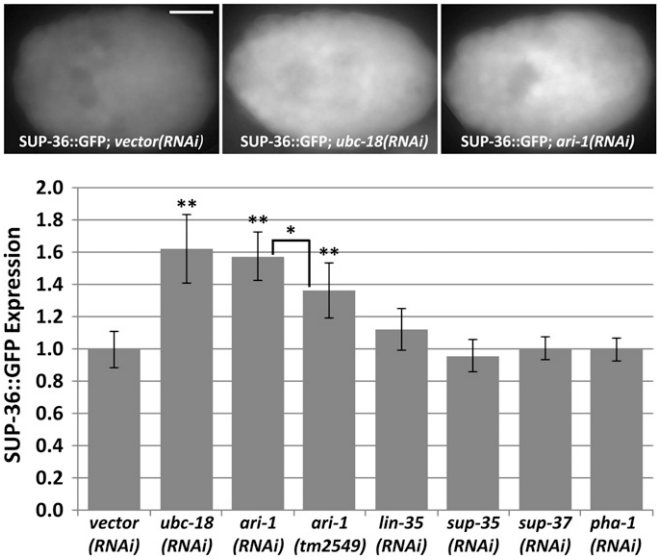

Figure 5 SUP-36::GFP expression regulation by upstream regulators. Expression levels of a full-length SUP-36::GFP reporter were assayed in embryos at the ~300-cell stage under the indicated conditions. Top panels show representative fluorescence images of wild-type, *ubc-18(RNAi)*, and *ari-1(RNAi)* embryos. Bottom panel shows quantification of embryos ($n > 50$ for each). Error bars indicate 95% confidence intervals (C.I.'s). Statistical analysis was carried out using Students *t*-test; $^{**}P < 0.001$ relative to vector control, $^{*}P < 0.05$. Bar, 10 μm.

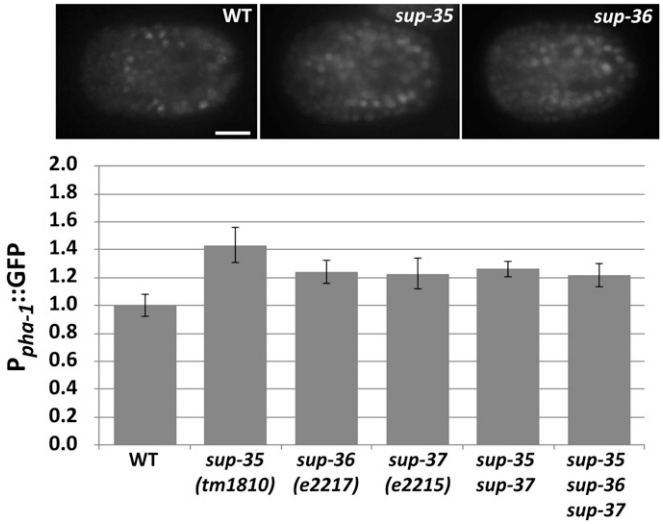

Figure 6 *pha-1* regulation by SUP-35, SUP-36, and SUP-37. Expression levels of a P_{pha-1}::GFP reporter were assayed in embryos at the ~300-cell stage under the indicated conditions. Error bars indicate 95% C.I.'s. $P < 0.05$ based on Student's *t*-test for all backgrounds relative to wild type.

2012). Consistent with this, we detected an ~1.4-fold increase in SUP-36::GFP in *ari-1(tm2549)* null deletion mutants (Figure 5). The somewhat lower fold change in expression observed in *ari-1(tm2549) vs. ari-1(RNAi)* mutants likely reflects the residual activities of the *ari-1* paralogs C27A12.6 and C27A12.7, whose expression is inhibited by *ari-1(RNAi)* through "off-target" effects (Qiu and Fay 2006). Thus, the three *ari-1*-like genes in *C. elegans* are likely to be partially redundant. Finally, SUP-36::GFP expression levels were not altered following reduction of *sup-35* or *sup-37* by RNAi (Figure 5).

Regulation of pha-1 expression by SUP-36

Both SUP-35 and SUP-37 negatively regulate *pha-1* expression at the level of transcription (Mani and Fay 2009; Fay *et al.* 2012). However, this regulation is relatively weak and cannot account for the ability of mutations in *sup-35* and *sup-37* to suppress null alleles of *pha-1* (Fay *et al.* 2012). Nevertheless, we examined *pha-1* expression in *sup-36* mutants to see whether *sup-36* may also negatively regulate *pha-1* transcription. Consistent with *sup-35* and *sup-37* mutants, *sup-36* mutants showed a small but statistically significant increase in the expression of a P_{pha-1}::GFP reporter (Figure 6), indicating that SUP-36 also plays some role in the regulation of *pha-1* expression. To test for additive effects, we examined compound mutants with *sup-36*, including a *sup-35*; *sup-36*; *sup-37* triple mutant. We failed, however, to observe enhanced effects on *pha-1* expression in compound mutants (Figure 6). The absence of any additive effects is consistent with the model that SUP-35/-36/-37 may act together as a functional unit.

Physical interactions between SUP-35, SUP-37, and SUP-36

Our genetic data and expression analyses suggested that SUP-35, SUP-36, and SUP-37 may physically interact, possibly within the context of a macromolecular complex or pathway. To further test this model, we assayed purified His-tagged SUP-35 for binding to *in vitro*-translated SUP-36 and SUP-37. SUP-37 coprecipitated with SUP-35 (Figure 7A), suggesting that these two Zn-finger proteins associate *in vivo*. In contrast, incubation of SUP-35 and SUP-36 did not lead to the coprecipitation of SUP-36 with SUP-35 (Figure 7A); this was also true for additional tests using a bacterially expressed GST–SUP-36 fusion protein (data not shown). Furthermore, incubation of both SUP-36 and SUP-37 with purified SUP-35 resulted in the coprecipitation of SUP-37 only (Figure 7A). These findings suggest that SUP-36 does not bind directly to either SUP-35 or SUP-37.

SUP-35 contains a conserved regulator of microtubule dynamics (RMD) domain (Mani and Fay 2009), which confers binding to microtubules (Oishi *et al.* 2007). To test whether SUP-35 can bind to microtubules, we used purified His-tagged SUP-35 in a microtubule pull-down assay. SUP-35 was consistently enriched within the microtubule-concentrated pellet fractions (Figure 7B). We note that our incubation conditions, which were necessary to maintain SUP-35 in a soluble form, slightly inhibited the enrichment of microtubules within the pelleted fraction relative to conditions used for our microtubule-binding (MAP2) and nonbinding (BSA) controls (Figure 7B). Nevertheless, the enrichment of SUP-35 within the pelleted fraction in the presence of microtubules indicates that SUP-35 binds to

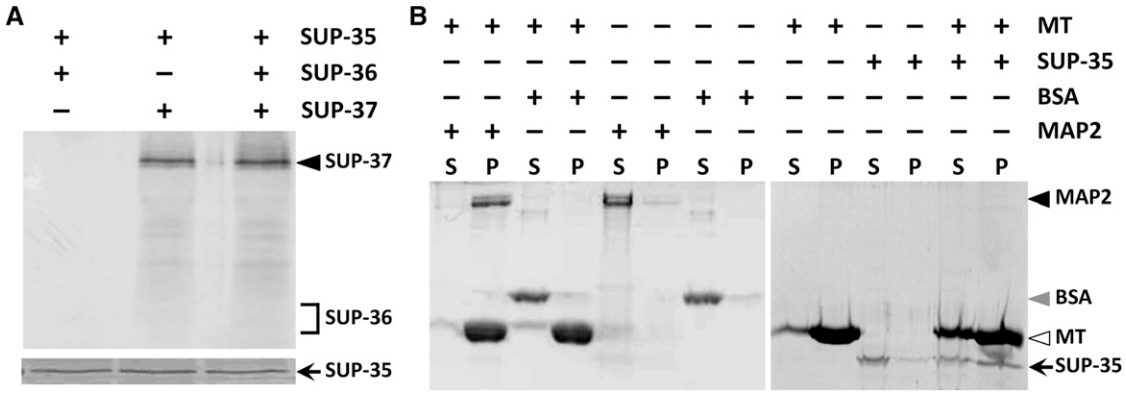

Figure 7 SUP-35 interacts with both SUP-37 and microtubules. (A) Coprecipitation experiments using purified full-length His-tagged SUP-35 and full-length ^{35}S-labeled SUP-36 and SUP-37 *in vitro*-translated proteins. The presence of correctly sized ^{35}S-labeled SUP-36 and SUP-37 was confirmed in separate experiments (data not shown). SUP-36 and SUP-37 were detected by autoradiography, whereas SUP-35 was detected by Coomassie staining. (B) Microtubule (MT) pull-down binding assays that were carried out using full-length His-tagged SUP-35 along with positive (MAP2) and negative (BSA) controls as indicated. Note that the large majority of SUP-35 is contained within the supernatant (S) in the absence of microtubules but is enriched in the pellet fraction (P) in the presence of microtubules.

microtubules and is consistent with the presence of an RMD domain in SUP-35. Interestingly, SUP-36 and PTL-1, the *C. elegans* ortholog of the mammalian microtubule-associated protein τ/MAP2/MAP4, display high-confidence interactions based on two-hybrid studies (Li *et al.* 2004; Simonis *et al.* 2009). Using independently generated SUP-36 bait and PTL-1 prey constructs, we have confirmed binding between SUP-36 and PTL-1 in the yeast system (Figure 3). It is therefore possible that PTL-1 and microtubules could bridge an association between SUP-35–SUP-37 and SUP-36.

SUP-35 is mislocalized in sup-36 mutants

Overexpression of SUP-35 or SUP-35::GFP can be toxic in a wild-type background (Mani and Fay 2009). For this reason, our previous analysis of SUP-35::GFP expression was carried out in a *sup-36* mutant background, in which SUP-35 overexpression was not toxic. More recently, we have been able to generate strains that express SUP-35::GFP in a wild-type background, which may be due to lower levels of SUP-35 expression from this array. SUP-35 expression in wild type and *sup-36* mutants was identical at early stages of development, in which the large majority of SUP-35::GFP is cytoplasmic (Figure 8, A and D). Beginning at the time of morphogenesis, however, significant differences in SUP-35::GFP localization were observed between wild type and *sup-36* mutants. Whereas SUP-35::GFP expression in wild type was punctate and largely confined to the region coinciding with the nuclear membrane or periphery, expression in *sup-36* mutants, as previously reported (Mani and Fay 2009), was predominantly nuclear. This suggests that SUP-36 may directly or indirectly regulate SUP-35 subcellular localization. We did not detect any obvious differences in the cell types that expressed SUP-35::GFP in wild type *vs.* *sup-36* mutants, suggesting that SUP-36 specifically regulates SUP-35 localization within the cell. To see whether SUP-36 expression may be regulated by SUP-35 or SUP-37, we examined SUP-36::GFP expression in wild type (Figure 4) and in the *sup-35(tm1810)*; *sup-36(e2217)*; *sup-37(e2215)* triple-mutant background (Figure S5), but we detected no obvious differences.

A whole-genome RNAi suppressor screen identifies transcriptional regulators and SCF components as mediators of pharyngeal development

In a saturating genetic screen carried out by Schnabel and colleagues, only three loci (*sup-35*, *sup-36*, and *sup-37*) were identified that could suppress *pha-1* LOF lethality (Schnabel *et al.* 1991). All three *pha-1* suppressors also suppress the synthetic-lethal phenotypes of *lin-35*; *ubc-18*, *lin-35*; *pha-1*, and *ari-1*; *pha-1* double mutants (Table 1) (Fay *et al.* 2004, 2012; Qiu and Fay 2006; Mani and Fay 2009). We reasoned, however, that additional regulators of this pharyngeal network are likely to exist and may be identified by their ability to suppress *lin-35*; *ubc-18* mutants, which display a less severe phenotype than do strong LOF *pha-1* mutants. We therefore carried out a whole-genome RNAi feeding screen for suppressors of *lin-35*; *ubc-18* synthetic lethality. In addition to finding several expected suppressors, such as *sup-35* and *sup-37*, we identified 39 additional clones that consistently suppressed *lin-35*; *ubc-18* larval arrest (Figure 9; Table S1). Whereas <5% of *lin-35*; *ubc-18* mutants normally bypassed larval arrest, the identified suppressors typically led to 20–50% of double mutants reaching the adult stage (Figure 9). Molecular descriptions of the suppressors are shown in Table S1. The single largest class of suppressors contains 23 genes and corresponds to many previously identified multiphenotypic *lin-35* suppressors (MPLS) (Polley and Fay 2012). These genes are thought to act antagonistically to LIN-35 and to regulate the expression of transcriptional targets at the level of chromatin structure (Cui *et al.* 2006b; Polley and Fay 2012). Our screen identified six new MPLS genes, including F26A1.1, which suppressed four distinct *lin-35*-synthetic phenotypes but not *lin-35*; *slr-2* and *lin-15a/b* (Figure S6), thus accounting for the absence of

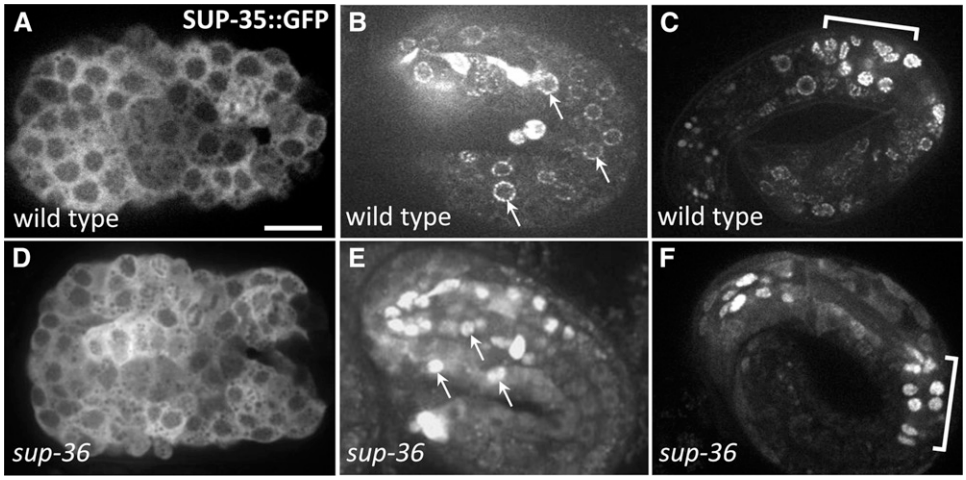

Figure 8 SUP-35::GFP localization is altered in *sup-36* mutants. (A–F) Confocal fluorescence images of full-length functional SUP-35::GFP in embryos. A and D show embryos prior to morphogenesis (~300–350 min postfertilization), B and E show twofold-stage embryos (~450 min), and C and F show approximately threefold-stage embryos (>600 min). Both wild-type and *sup-36 (e2217)* strains contained the same SUP-35::GFP extrachromosomal array (*fdEx57*). Arrows in B and E indicate the positions of nuclei. Brackets in C and F indicate the region containing posterior pharyngeal cells. Bar in A, 10 μm for A–F.

this gene from previous suppressor screens. Somewhat surprisingly, most *lin-35*; *ubc-18* suppressors failed to significantly suppress the phenotypically related synthetic lethality of *lin-35*; *pha-1(fd1)* mutants (Figure S6 and data not shown). This may be attributable to the somewhat stronger and more highly penetrant phenotype of *lin-35*; *pha-1* double mutants (Fay *et al.* 2004), a conclusion that is consistent with results obtained from the analysis of MPLS genes identified through a *lin-35*; *slr-2* suppressor screen (Polley and Fay 2012). Furthermore, a small-scale *lin-35*; *pha-1* RNAi suppressor screen failed to identify suppressors that were distinct from those identified by the *lin-35*; *ubc-18* screen (data not shown).

The *lin-35*; *ubc-18* suppressor screen also identified four putative regulators of transcription that are not MPLS genes (Figure 9). Two of these genes, *met-2/SETDB1* and *lin-61/L(3)MBTL2*, were previously identified as class B SynMuv genes (Poulin *et al.* 2005; Harrison *et al.* 2007). The **sy**nthetic **mu**lti**v**ulval (SynMuv) phenotype is produced by mutations in two genes (one class A gene and one class B gene) that act redundantly to inhibit the formation of multiple vulval structures (Fay and Yochem 2007). (Wild-type hermaphrodite worms have but one vulva.) Class B SynMuv genes function redundantly with class A SynMuv genes to repress the expression of LIN-3/EGF in the hypodermis (Cui *et al.* 2006a; Fay and Yochem 2007). Class B SynMuv genes include LIN-35/pRb and its binding partner EFL-1/E2F (Lu and Horvitz 1998). Notably, many class B SynMuv genes are conserved in mammals and function within several structurally related transcriptional repressor complexes (Fay and Yochem 2007; van den Heuvel and Dyson 2008). LIN-61 contains four malignant brain tumor (MBT) repeats, which bind to modified histones and are found in transcriptional repressors including the Polycomb-group proteins (Harrison *et al.* 2007; Bonasio *et al.* 2010). LIN-61 binds to histone H3 when this protein is di- or trimethylated on lysine 9 (Koester-Eiserfunke and Fischle 2011). Correspondingly, MET-2 is a histone-methyltransferase that promotes H3K9 dimethylation (Andersen and Horvitz 2007; Bessler *et al.* 2010; Towbin *et al.* 2012). Thus, LIN-61 and MET-2 are closely linked functionally and together promote transcriptional repression. This differs from the proposed mode of action for MPLS genes, which are thought to act primarily as transcriptional activators (Cui *et al.* 2006a; Petrella *et al.* 2011; Xiao *et al.* 2011; Polley and Fay 2012). The identification of class B SynMuv genes as suppressors of a *lin-35*-synthetic phenotype was somewhat surprising given that in the context of LIN-3 regulation, class B SynMuv genes act in concert with each other and in some cases can even show enhancer-type interactions (Andersen *et al.* 2008).

Another class of *lin-35*; *ubc-18* suppressors includes genes that encode putative components of SCF complexes. This includes one RNAi clone that targets the closely related Skp1 family members *skr*-8 and *skr-9* as well as a separate RNAi clone that targets both *skr-12* and *skr-13* (Figure 9). A third clone targets K06H7.2, which encodes an F-box protein. Given that *sup-36* encodes a protein that is related to Skp1 family members, suppression by SCF-type clones may occur through a mechanism that is related to suppression by *sup-36*. This is consistent with these clones not suppressing unrelated *lin-35*-synthetic phenotypes. The identification of SCF components as suppressors of *lin-35*; *ubc-18* further supports the hypothesis that the molecular function of SUP-36 is linked to that of other Skp1 family members.

Discussion

Our collective findings support the model for pharyngeal development depicted in Figure 10. In this model, LIN-35–EFL-1, which forms a transcriptional repressor complex, and HCF-1, which acts as a positive transcriptional regulator, mutually control the expression levels of *sup-35* mRNA (Mani and Fay 2009; Fay *et al.* 2012). Direct control of SUP-35 expression by these upstream factors is further supported by the recent finding that LIN-35 associates with the promoter of SUP-35 *in vivo* (Kudron *et al.* 2013). In addition, ARI-1–UBC-18 negatively regulates both SUP-35 and SUP-36 post-translationally, presumably through ubiquitin-mediated proteolysis (Figure 5) (Mani and Fay 2009). Thus, in *lin-35*; *ubc-18* double mutants, levels of both SUP-35 and

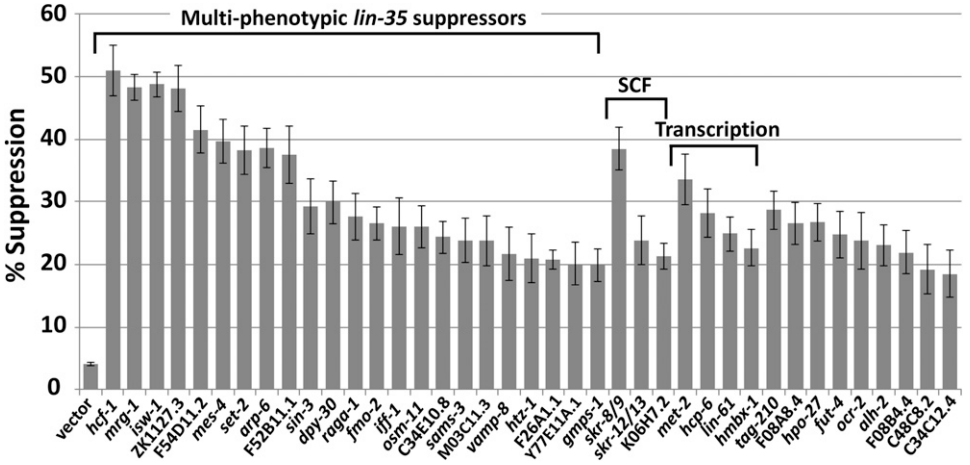

Figure 9 *lin-35*; *ubc-18* suppressors identified by a whole-genome RNAi screen. Shown is percentage of suppression of larval arrest by 39 sequence-confirmed RNAi clones. Vector denotes a control RNAi. Suppressors have been organized into functional classes. The six new multiphenotypic *lin-35* suppressor genes that were identified are *arp-6*, *fmo-2*, *vamp-8*, F26A1.1, Y77E11A.1, and *gmps-1*. Error bars indicate 95% C.I.'s. For all suppressor RNAi clones, $P < 0.001$ (relative to vector control) based on the exact test.

SUP-36 are elevated, which then interferes with PHA-1 activity. Consistent with this, overexpression of either SUP-35 or SUP-36 leads to *pha-1* LOF phenotypes in a genetic background in which *pha-1* activity is partially compromised, *i.e.*, *pha-1(ts)* at 16° (Figure 1D) (Mani and Fay 2009). In addition, SUP-35/-36/-37 negatively regulate *pha-1* at the level of transcription, although this effect is weak (Figure 6). Finally, separate from its role with SUP-35 and SUP-36 in opposing PHA-1 functions, SUP-37 functions independently to regulate pharyngeal pumping and ovulation (Fay *et al.* 2012). We note that the hypothesized common target of SUP-35/-36/-37 and PHA-1 is not currently known, nor is the basic molecular function of PHA-1 understood.

Our observation that purified SUP-35 and SUP-37 directly associated (Figure 7A) supports a model whereby these proteins function as a dimer, possibly within the context of a larger protein complex. Although SUP-36 did not bind directly to either SUP-35 or SUP-37 in our assays, SUP-36 bound to the conserved microtubule-associated protein PTL-1/τ in Y2H assays (Figure 3) (Li *et al.* 2004; Simonis *et al.* 2009). Based on our finding that SUP-35 bound directly to microtubules (Figure 7B; likely via the RMD domain), we speculate that SUP-35/-36/-37 may be capable of forming a macromolecular complex, with cytoskeletal components bridging the connection between SUP-35–SUP-37 and SUP-36 (Figure 10). Complex formation by SUP-35/-36/-37 is also largely consistent with genetic and phenotypic data, as well as with their coexpression during certain stages of embryogenesis (Mani and Fay 2009; Fay *et al.* 2012). Nevertheless it is important to point out that although two-way binding between various components (*e.g.*, SUP-35–SUP-37 and SUP-35–microtubules) was demonstrated (Figure 3 and Figure 7), it is unknown whether simultaneous interactions between multiple components occur. In addition, other possibilities for functional relationships exist, as suggested by the observation that SUP-36 may regulate the subcellular localization of SUP-35 (Figure 8). Furthermore, the SUPs are likely to have functions that are independent of each other. For example, SUP-37 functions independently of SUP-35 and SUP-36 to promote pharyngeal pumping and somatic gonad functions (Fay *et al.* 2012). Thus, although complex formation between the SUPs may occur, it is unlikely to account for all of their activities.

We have confirmed that SUP-36 binds to at least two *C. elegans* F-box proteins (FBXC-20 and FBXC-53) and was reported to bind to a third (FBXC-32) based on Y2H assays (Figure 3) (Li *et al.* 2004; Simonis *et al.* 2009). This finding is consistent with SUP-36 functioning as a Skp1 family member and supports the idea that SUP-36 is a component of SCF complexes and may function in protein ubiquitylation. Although all three F-box proteins are expressed during embryogenesis, their specific functions are currently unknown (Levin *et al.* 2012). Although RNAi of these genes failed to suppress either *pha-1* or *lin-35*; *ubc-18* mutants (data not shown), there is likely to be a high degree of genetic redundancy among F-box proteins in *C. elegans*, thereby making their functional analysis difficult. For example, whereas the human and *Drosophila melanogaster* genomes are predicted to encode 38 and 22 F-box proteins, respectively, *C. elegans* is predicted to encode 322 (Kipreos and Pagano 2000). Our finding that SUP-36 can regulate SUP-35::GFP subcellular localization suggests that SUP-35 could be a target of SUP-36-mediated ubiquitylation, which is also consistent

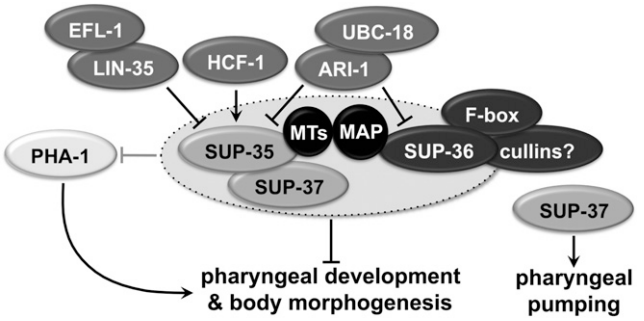

Figure 10 Model of pharyngeal regulation. Although binding between various binary components such as SUP-35–SUP-37 and SUP-35–microtubules was demonstrated by experimentation, it is unknown whether simultaneous interactions between multiple components also occur. For additional details, see text.

with our observation that SUP-35 is ubiquitylated *in vivo* (Mani and Fay 2009). Notably, ubiquitin modification is known to regulate the nuclear export of multiple mammalian proteins including p53, DCN1, RUNX3, and SHMT1 (Lohrum *et al.* 2001; Chi *et al.* 2009; Wu *et al.* 2011; Anderson *et al.* 2012).

In addition to SUP-35/-36/-37, our genome-wide *lin-35*; *ubc-18* RNAi suppressor screen identified 39 genes whose activities integrate with the described network to regulate pharyngeal development (Figure 9). Based on their ability to suppress multiple independent *lin-35*-synthetic phenotypes, the majority of suppressors are likely to act in a manner that directly opposes LIN-35 functions. Namely, MPLS genes may be positive regulators of targets that are globally repressed by LIN-35. Somewhat to our surprise, we also identified two class B SynMuv genes, LIN-61 and MET-2, which act through histone modification and binding to repress transcription. Like LIN-35, LIN-61 and MET-2 repress LIN-3/EGF expression in conjunction with class A SynMuv genes (Cui *et al.* 2006a; Andersen and Horvitz 2007). Unlike LIN-35 and EFL-1, however, LIN-61 and MET-2 are not core components of the *C. elegans* DP–Rb–class B SynMuv (DRM) complex in *C. elegans* (Harrison *et al.* 2007). We therefore hypothesize that LIN-61 and MET-2 may regulate some other node within the network (*e.g.*, *ubc-18* or *ari-1*), thereby accounting for their ability to repress the synthetic phenotype when inhibited. Finally, our identification of several SCF components is consistent with SUP-36 functioning as a Skp1-like protein (Figure 9).

Although the regulatory network and genes that we have identified are likely to be fairly comprehensive, a number of key questions remain, including the basic cellular function of PHA-1 and the means by which SUP-35/-36/-37 and PHA-1 oppose each other's activities. In addition, the meaning behind the dynamic expression patterns of SUP-35 and SUP-36 is unknown, as is the role that the microtubule cytoskeleton might play in either SUP-35/-36/-37 localization or function. Therefore future studies will be required to clarify the mechanistic details of this gene network.

Acknowledgements

We thank Amy Fluet from BiomEditor for editing and Ralf Schnabel and the *Caenorhabditis* Genetics Center for providing strains. Aleksandra Kuzmanov was supported by Wyoming IDeA Networks for Biomedical Excellence (INBRE) grant P20 GM103432. This work was supported by grant GM066868 from the National Institutes of Health.

Literature Cited

Ahringer, J., 2005 Reverse genetics (April 6, 2006), *WormBook*, ed. The *C. elegans* Research Community, WormBook, doi/10.1895/wormbook.1.47.1, http://www.wormbook.org.

Andersen, E. C., and H. R. Horvitz, 2007 Two C. elegans histone methyltransferases repress lin-3 EGF transcription to inhibit vulval development. Development 134: 2991–2999.

Andersen, E. C., A. M. Saffer, and H. R. Horvitz, 2008 Multiple levels of redundant processes inhibit *Caenorhabditis elegans* vulval cell fates. Genetics 179: 2001–2012.

Anderson, D. D., J. Y. Eom, and P. J. Stover, 2012 Competition between sumoylation and ubiquitination of serine hydroxymethyltransferase 1 determines its nuclear localization and its accumulation in the nucleus. J. Biol. Chem. 287: 4790–4799.

Bessler, J. B., E. C. Andersen, and A. M. Villeneuve, 2010 Differential localization and independent acquisition of the H3K9me2 and H3K9me3 chromatin modifications in the Caenorhabditis elegans adult germ line. PLoS Genet. 6: e1000830.

Blumenthal, T., and K. Steward, 1997 RNA processing and gene structure, pp. 117–145 in *C. elegans II*, edited by D. L. Riddle, T. Blumenthal, B. J. Meyer, and J. R. Priess. Cold Spring Harbor Laboratory Press, Plainview, NY.

Bonasio, R., E. Lecona, and D. Reinberg, 2010 MBT domain proteins in development and disease. Semin. Cell Dev. Biol. 21: 221–230.

Chi, X. Z., J. Kim, Y. H. Lee, J. W. Lee, K. S. Lee *et al.*, 2009 Runt-related transcription factor RUNX3 is a target of MDM2-mediated ubiquitination. Cancer Res. 69: 8111–8119.

Cui, M., J. Chen, T. R. Myers, B. J. Hwang, P. W. Sternberg *et al.*, 2006a SynMuv genes redundantly inhibit lin-3/EGF expression to prevent inappropriate vulval induction in C. elegans. Dev. Cell 10: 667–672.

Cui, M., E. B. Kim, and M. Han, 2006b Diverse chromatin remodeling genes antagonize the Rb-involved SynMuv pathways in C. elegans. PLoS Genet. 2: e74.

Deshaies, R. J., 1999 SCF and Cullin/Ring H2-based ubiquitin ligases. Annu. Rev. Cell Dev. Biol. 15: 435–467.

Fay, D., 2006 Genetic mapping and manipulation: chapter 5–SNPs: three-point mapping (February 17, 2006), *WormBook*, ed. The *C. elegans* Research Community, WormBook, doi/10.1895/wormbook.1.94.1, http://www.wormbook.org.

Fay, D. S., and J. Yochem, 2007 The SynMuv genes of Caenorhabditis elegans in vulval development and beyond. Dev. Biol. 306: 1–9.

Fay, D. S., E. Large, M. Han, and M. Darland, 2003 lin-35/Rb and ubc-18, an E2 ubiquitin-conjugating enzyme, function redundantly to control pharyngeal morphogenesis in C. elegans. Development 130: 3319–3330.

Fay, D. S., X. Qiu, E. Large, C. P. Smith, S. Mango *et al.*, 2004 The coordinate regulation of pharyngeal development in C. elegans by lin-35/Rb, pha-1, and ubc-18. Dev. Biol. 271: 11–25.

Fay, D. S., S. R. Polley, J. Kuang, A. Kuzmanov, J. W. Hazel *et al.*, 2012 A regulatory module controlling pharyngeal development and function in *Caenorhabditis elegans*. Genetics 191: 827–843.

Granato, M., H. Schnabel, and R. Schnabel, 1994 Genesis of an organ: molecular analysis of the pha-1 gene. Development 120: 3005–3017.

Harrison, M. M., X. Lu, and H. R. Horvitz, 2007 LIN-61, one of two *Caenorhabditis elegans* malignant-brain-tumor-repeat-containing proteins, acts with the DRM and NuRD-like protein complexes in vulval development but not in certain other biological processes. Genetics 176: 255–271.

Kipreos, E. T., 2005 Ubiquitin-mediated pathways in C. elegans (December 01, 2005), *WormBook*, ed. The *C. elegans* Research Community, WormBook, doi/10.1895/wormbook.1.36.1, http://www.wormbook.org.

Kipreos, E. T., and M. Pagano, 2000 The F-box protein family. Genome Biol. 1(5): REVIEWS3002.

Koester-Eiserfunke, N., and W. Fischle, 2011 H3K9me2/3 binding of the MBT domain protein LIN-61 is essential for Caenorhabditis elegans vulva development. PLoS Genet. 7: e1002017.

Kudron, M., W. Niu, Z. Lu, G. Wang, M. Gerstein *et al.*, 2013 Tissue-specific direct targets of Caenorhabditis elegans Rb/E2F dictate distinct somatic and germline programs. Genome Biol. 14: R5.

Levin, M., T. Hashimshony, F. Wagner, and I. Yanai, 2012 Developmental milestones punctuate gene expression in the Caenorhabditis embryo. Dev. Cell 22: 1101–1108.

Li, S., C. M. Armstrong, N. Bertin, H. Ge, S. Milstein *et al.*, 2004 A map of the interactome network of the metazoan C. elegans. Science 303: 540–543.

Lohrum, M. A., D. B. Woods, R. L. Ludwig, E. Balint, and K. H. Vousden, 2001 C-terminal ubiquitination of p53 contributes to nuclear export. Mol. Cell. Biol. 21: 8521–8532.

Lu, X., and H. R. Horvitz, 1998 lin-35 and lin-53, two genes that antagonize a C. elegans Ras pathway, encode proteins similar to Rb and its binding protein RbAp48. Cell 95: 981–991.

Mani, K., and D. S. Fay, 2009 A mechanistic basis for the coordinated regulation of pharyngeal morphogenesis in Caenorhabditis elegans by LIN-35/Rb and UBC-18-ARI-1. PLoS Genet. 5: e1000510.

Oishi, K., H. Okano, and H. Sawa, 2007 RMD-1, a novel microtubule-associated protein, functions in chromosome segregation in Caenorhabditis elegans. J. Cell Biol. 179: 1149–1162.

Petrella, L. N., W. Wang, C. A. Spike, A. Rechtsteiner, V. Reinke *et al.*, 2011 synMuv B proteins antagonize germline fate in the intestine and ensure C. elegans survival. Development 138: 1069–1079.

Polley, S. R., and D. S. Fay, 2012 A network of genes antagonistic to the LIN-35 retinoblastoma protein of *Caenorhabditis elegans*. Genetics 191: 1367–1380.

Portereiko, M. F., and S. E. Mango, 2001 Early morphogenesis of the Caenorhabditis elegans pharynx. Dev. Biol. 233: 482–494.

Portereiko, M. F., J. Saam, and S. E. Mango, 2004 ZEN-4/MKLP1 is required to polarize the foregut epithelium. Curr. Biol. 14: 932–941.

Poulin, G., Y. Dong, A. G. Fraser, N. A. Hopper, and J. Ahringer, 2005 Chromatin regulation and sumoylation in the inhibition of Ras-induced vulval development in Caenorhabditis elegans. EMBO J. 24: 2613–2623.

Qiu, X., and D. S. Fay, 2006 ARI-1, an RBR family ubiquitin-ligase, functions with UBC-18 to regulate pharyngeal development in C. elegans. Dev. Biol. 291: 239–252.

Schnabel, H., and R. Schnabel, 1990 An organ-specific differentiation gene, pha-1, from Caenorhabditis elegans. Science 250: 686–688.

Schnabel, H., G. Bauer, and R. Schnabel, 1991 Suppressors of the organ-specific differentiation gene pha-1 of *Caenorhabditis elegans*. Genetics 129: 69–77.

Simonis, N., J. F. Rual, A. R. Carvunis, M. Tasan, I. Lemmens *et al.*, 2009 Empirically controlled mapping of the Caenorhabditis elegans protein-protein interactome network. Nat. Methods 6: 47–54.

Stiernagle, T., 2005 Maintenance of C. elegans (February 11, 2006), *WormBook*, ed. The *C. elegans* Research Community, WormBook, doi/10.1895/wormbook.1.101.1, http://www.wormbook.org.

Towbin, B. D., C. Gonzalez-Aguilera, R. Sack, D. Gaidatzis, V. Kalck *et al.*, 2012 Step-wise methylation of histone H3K9 positions heterochromatin at the nuclear periphery. Cell 150: 934–947.

van den Heuvel, S., and N. J. Dyson, 2008 Conserved functions of the pRB and E2F families. Nat. Rev. Mol. Cell Biol. 9: 713–724.

Willems, A. R., M. Schwab, and M. Tyers, 2004 A hitchhiker's guide to the cullin ubiquitin ligases: SCF and its kin. Biochim. Biophys. Acta 1695: 133–170.

Wu, K., H. Yan, L. Fang, X. Wang, C. Pfleger *et al.*, 2011 Monoubiquitination drives nuclear export of the human DCN1-like protein hDCNL1. J. Biol. Chem. 286: 34060–34070.

Xiao, Y., C. Bedet, V. J. Robert, T. Simonet, S. Dunkelbarger *et al.*, 2011 *Caenorhabditis elegans* chromatin-associated proteins SET-2 and ASH-2 are differentially required for histone H3 Lys 4 methylation in embryos and adult germ cells. Proc. Natl. Acad. Sci. USA 108: 8305–8310.

Communicating editor: P. Sengupta

GENETICS

Supporting Information
http://www.genetics.org/lookup/suppl/doi:10.1534/genetics.113.158485/-/DC1

Implicating SCF Complexes in Organogenesis in *Caenorhabditis elegans*

Stanley R. G. Polley, Aleksandra Kuzmanov, Jujiao Kuang, Jonathan Karpel, Vladimir Lažetić, Evguenia I. Karina, Bethany L. Veo, and David S. Fay

DOI: 10.1534/genetics.113.158485

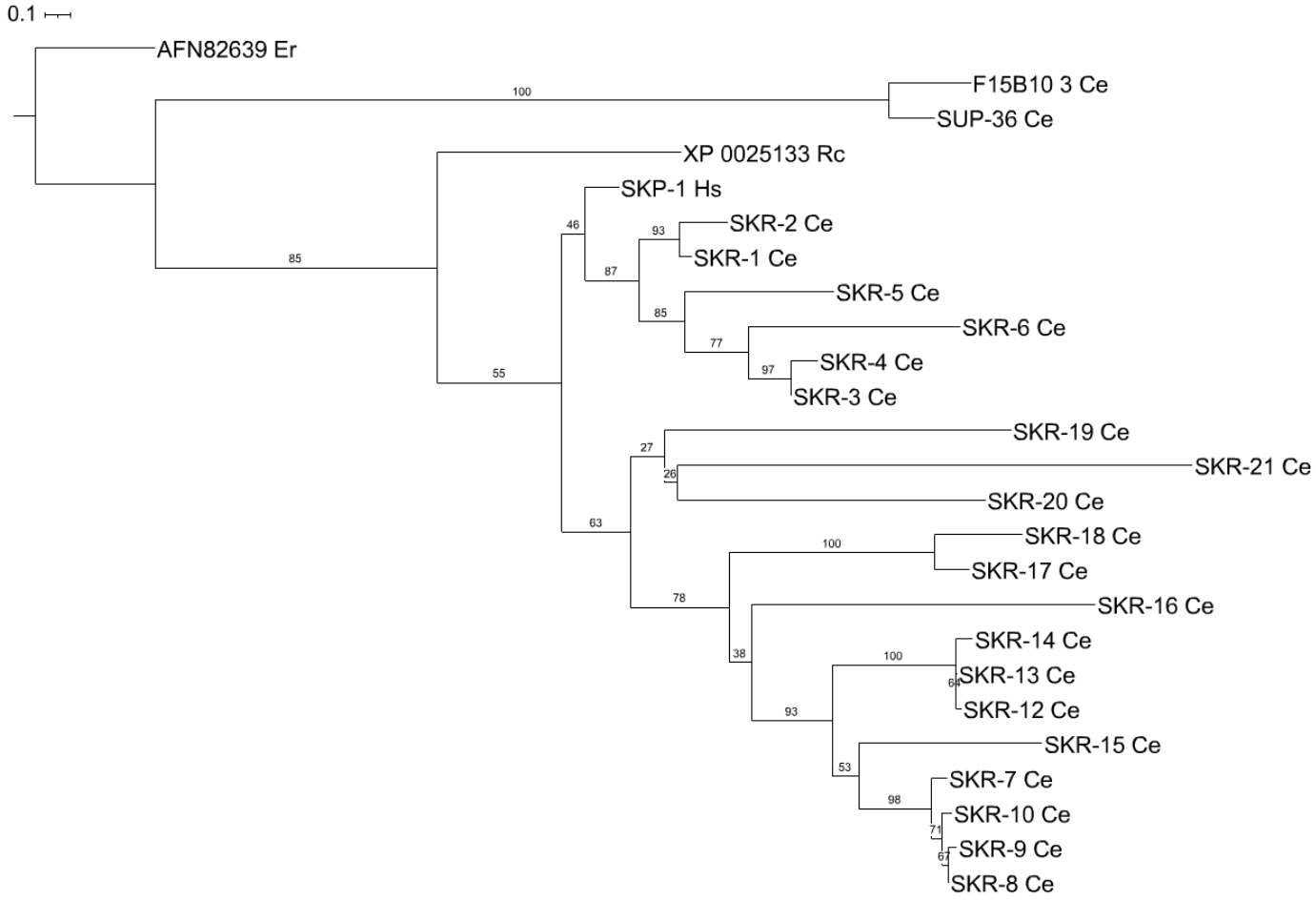

Figure S1 Dendrogram of SUP-36 and Skp1 family members. The dendrogram was generated using MAFFT alignment. AFN82639 and XP_002513359 are Skp1-like proteins from ***Encephalitozoon romaleae*** **(Er;** microsporidia) **and** *Ricinus communis* (Rc; castor bean), respectively. Spk1 is from *Homo sapiens* (Hs). All other proteins are from *C. elegans* (Ce). Scale bar indicates branch length; numbers indicate bootstraps (out of 100) that supported the displayed branch configuration.

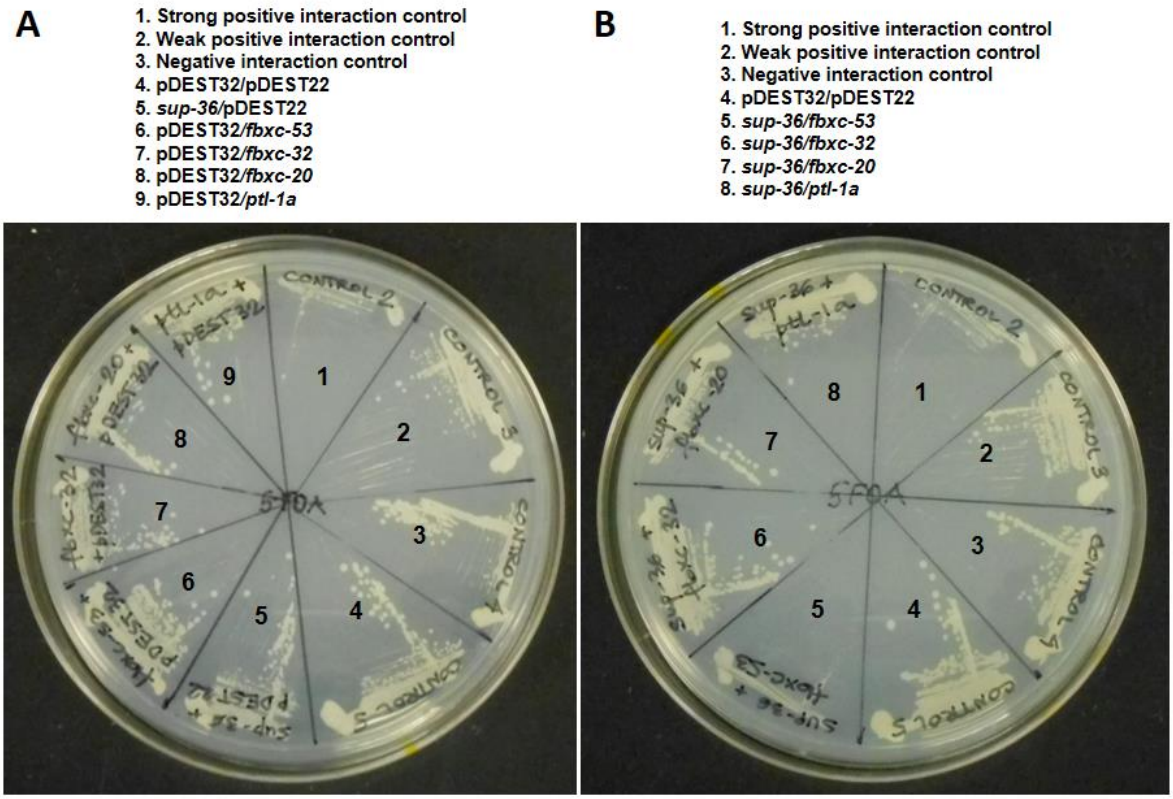

Figure S2 Growth of indicated yeast strains on 5-FOA plates. (A) Observed induction of the *URA3* reporter gene in the negative activation controls (*sup-36* bait with empty prey vector [pDEST22] and prey clones [*fbxc-53, fbxc-32, fbxc-20*, and *ptl-1a*] with empty bait vector [pDEST32]). (B) Yeast strains co-transformed with *sup-36* bait and each of the prey clones. Candidate yeast colonies were streaked onto 0.2% 5-FOA selection plates, and the extent of growth was determined after 72 hr. Reduced colony size and density on 5-FOA plates indicates activation of the *URA3* reporter gene. Strong, weak, and negative interaction controls were supplied by Invitrogen.

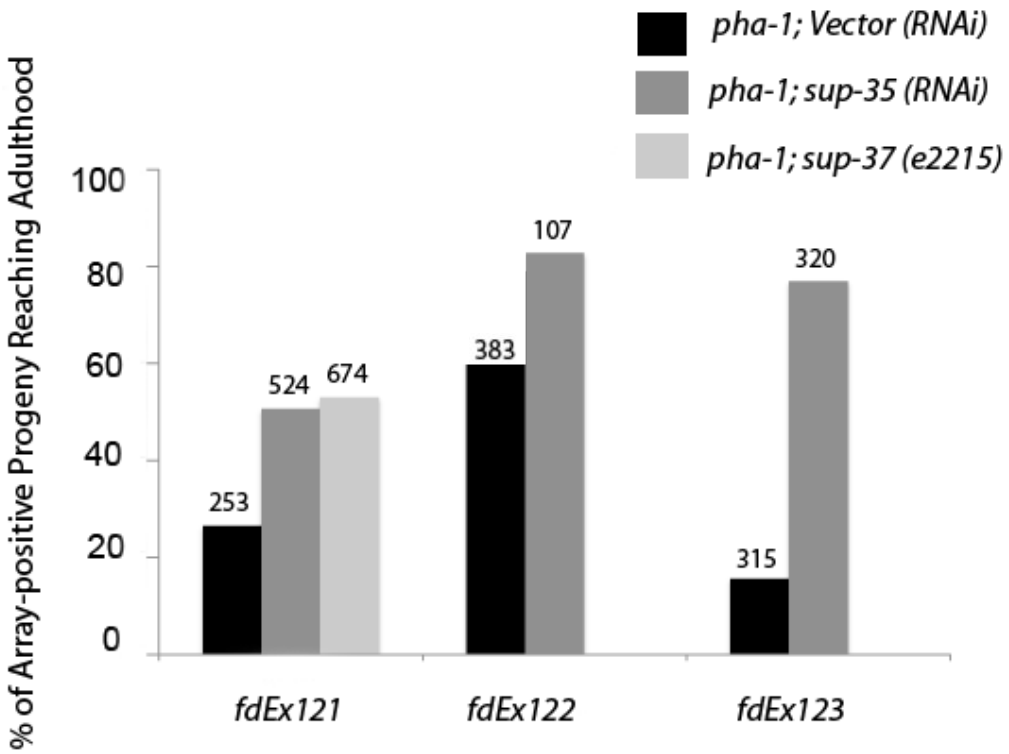

Figure S3 *sup-36* overexpression toxicity in *pha-1(e2123ts)* mutants at 16°C is suppressed by inhibition of *sup-35* and *sup-37*. Three strains (WY729–31) that carry independent multi-copy extrachromosomal arrays (*fdEx121–123*) containing the *sup-36* genomic locus in the *pha-1(ts)* background were assayed for toxicity at 16°C. Such strains typically produced a notable percentage of GFP+ (array-plus) progeny that arrest as embryos or L1 larvae with phenotypes that resemble *pha-1* LOF mutants. The percentage of GFP-positive F_1 progeny from GFP-positive P_0 mothers was scored when strains were grown on either vector control RNAi plates or *sup-35(RNAi)* plates. Notably, the percentage of array-positive adult progeny increased significantly ($p < 0.01$) for all three strains when they were grown on *sup-35(RNAi)* feeding plates as compared with those grown on control plates, indicating that inhibition of *sup-35* suppresses the toxicity of SUP-36 overexpression. We also generated a *pha-1(ts); sup-37(e2215); fdEx121* strain in which the percentage of viable adult progeny increased from ~25% to ~50% relative to *pha-1(ts); Vector(RNAi); fdEx121* ($p < 0.01$). Thus, a reduction in *sup-37* activity also suppressed the toxicity of SUP-36 overexpression. Numbers above each bar indicate the total number of animals scored under each condition.

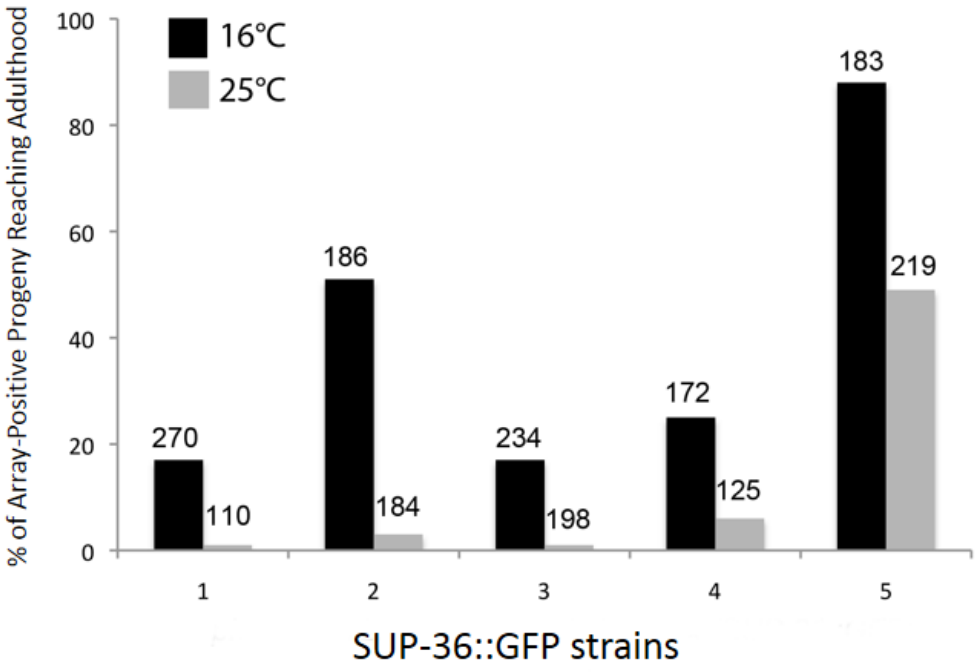

Figure S4 A SUP-36::GFP reporter is biologically active. Five independent extrachromosomal arrays expressing SUP-36::GFP were generated in *pha-1(e2123ts); sup-36(e2217)* mutants. To test for activity of the GFP fusion protein, we assayed the percentage of array-positive animals that reached adulthood for each line at the permissive (16°C) and non-permissive (25°C) temperatures for *pha-1(ts)*. In all cases, the viability of array-positive animals was dramatically reduced at the non-permissive temperature of 25°C in animals carrying the SUP-36::GFP reporter ($P < 0.01$).

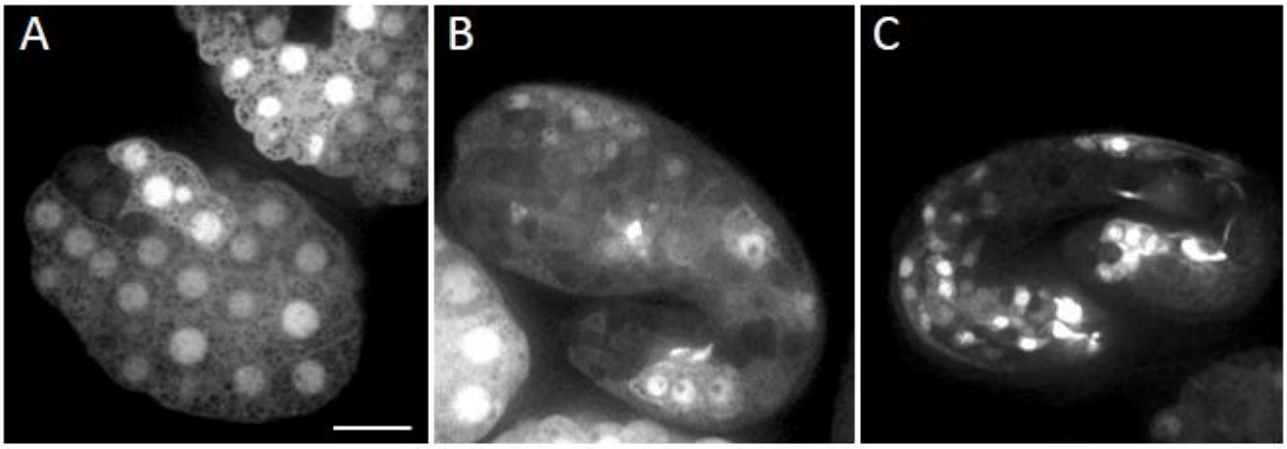

Figure S5 SUP-36::GFP expression is not altered in *sup-35; sup-37* mutants. SUP-36::GFP expression was examined in the triple-mutant strain WY1000 [*sup-35(tm1810) III; sup-36(e2217) IV; sup-37(e2215) V; fdEx235*]. No obvious differences in localization were detected in (A) early-stage (B) 1.5-fold-stage or (C) late-stage embryos with SUP-36::GFP expression between WY1000 and wild-type embryos (compare with Figure 4). Scale bar in A is 10 μm for A–C.

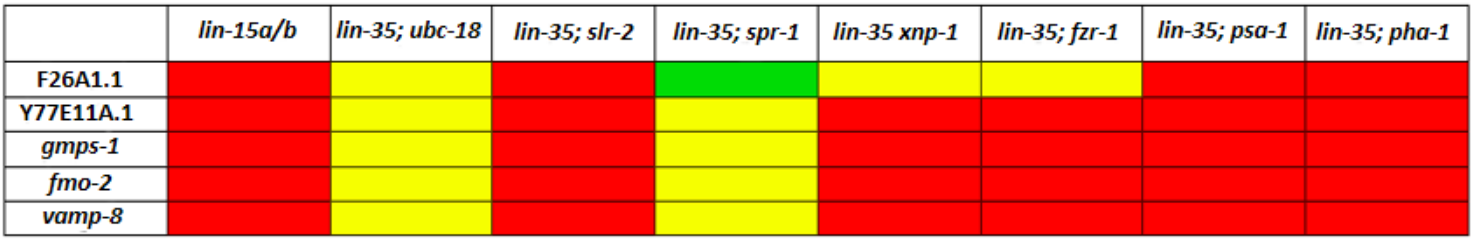

Figure S6 Suppression of multiple *lin-35*–synthetic phenotypes by RNAi clones. Suppression by RNAi clones (left-most column) of the indicated genotypes (top row) was scored as negative (red), moderate (yellow; 10–30% suppression), and strong (green; >30–100% suppression). All suppression values were normalized to the vector control RNAi values for each given genotype. Of the 39 RNAi clones identified on the basis of *lin-35; ubc-18* suppression, five previously uncharacterized MPLS genes were identified that suppressed at least two *lin-35*–synthetic phenotypes.

Table S1 Gene identities of *lin-35; ubc-18* suppressors

Genes sorted by category	Relevant ortholog/*C. elegans* functions/InterPro domain prediction
Multi-phenotypic *lin-35* suppressors (MPLS)	
hcf-1	Human host cell factor C1, methyltransferase complex member/life span as a DAF-16 regulator, histone modification/fibronectin III-like domain
mrg-1	Human TF MRG15/primordial germ cell survival, autosome associated, transcriptional regulator of germ and somatic tissue/chromodomain
isw-1	Yeast Isw2 ATP-dependent DNA translocase involved in chromatin remodeling/chromatin remodeling protein likely acting as ATPase component of nucleosome remodeling factor (NURF) complex/SANT, helicase
ZK1127.3	Human Tip60 HAT complex member/synMuv suppressor, MPLS gene/ novel
F54D11.2	Yeast GPI-anchored cell surface glycoprotein/SynMuv suppressor/novel
mes-4	Yeast Set2/Set1 H3K4-like methyltransferase, transcriptional activation of autosomes, dosage compensation, MPLS gene/SET domain, Zn-finger ring type
set-2	Yeast Set1 Histone H3K4 methyltransferase/embryogenesis, germline development, and lifespan/SET domain
arp-6	Yeast Arp6 actin-related protein component of the SWR1 component/synMuv suppressor/novel
F52B11.1	Human CpG binding protein/SynMuv suppressor/novel
sin-3	Yeast histone deacetylase Sin3/histone-silencing deacetylase, male development/glutamine + asparagine-rich domain, PAH domain
dpy-30	Human Set1 H3K4 methyltransferase–interacting member DPY30/SDC complex member, NOX-1 complex member/novel

raga-1	Human Ras-related GTPase RagA and RagB/Rag GTPase, life span, TOR pathway regulator/novel
iff-1	Yeast translation elongation factor eIF-5A/P-granule component localization, germ-cell proliferation/novel
osm-11	Nematode-specific/osmosensation, osmotic resistance, defecation rhythm/novel
C34E10.8	Yeast Muc1 GPI-anchored glycoprotein transcriptionally regulated by the MAPK pathway/DNA-binding domain
sams-3	Yeast Sam1 *S*-adenosylmethionine synthetase/longevity, *S*-adenosylmethionine synthetase/*S*-adenosylmethionine synthetase domains
M03C11.3	Nematode-specific/SynMuv suppressor/novel
htz-1	Human H2A.Z/Histone variant functions with FoxA transcription factor and MYS-1 and SWR1 remodeling complex to control transcription during pharynx development/histone core, histone fold
vamp-8	Human VAMP8 vesicle membrane receptor protein (v-SNARE)/uncharacterized gene/synaptobrevin domain
F26A1.1	Nematode-specific/uncharacterized gene/novel
gmps-1	Human GMPS**,** GMP synthetase/uncharacterized gene/GMP synthetase domain, Rossmann-like $\alpha/\beta/\alpha$ sandwich fold
Y77E11A.1	Yeast Hxk1 hexokinase, phosphorylates glucose/uncharacterized/hexokinase domain

fmo-2	Yeast Fmo1 flavin-containing monoxygenase/monoxygenase/flavin monoxygenase domains
SCF complex members	
skr-8/9	Yeast Skp1**,** the ubiquitin ligase SCF complex/lifespan/BTB/POZ fold, E3 ubiquitin ligase
skr-12/13	Yeast Skp1**,** the ubiquitin ligase SCF complex/lifespan/BTB/POZ fold, E3 ubiquitin ligase
K06H7.2	Nematode-specific/uncharacterized/F-Box domain, F-box associated domain
Transcriptional regulators	
met-2	Yeast Set2 histone methyltransferase/H3K9 and H3K36 methyltransferase, SynMuv B gene, lin-3 negative regulator/SET domain, Pre-SET domain, Post-SET domain, DNA binding domain
hcp-6	Human condensing-2 complex member/DNA condensation, microtubule binding to kinetochore, chromosome alignment/armadillo-like fold
lin-61	Human MBT-like protein/transcriptional repression complex member, binds H3K9m2/3 sites, Class B SynMuv gene/MBT repeat
hmbx-1	Human HMBOX/asymmetric gene expression in olfactory neurons/homeodomain
Other	
tag-210	Yeast Ola1 ATPase/uncharacterized/GTP binding domain, β-grasp domain, TGS-like domain
F08A8.4	Human peroxisomal acyl-coenzyme A oxidase/uncharacterized gene/acyl-CoA oxidase domain

hpo-27	Human uncharacterized gene/uncharacterized gene/armadillo-type fold
fut-4	Human FUT6 fucosyltransferase/glycosyltransferase /glycosyltransferase family 10
ocr-2	Human TRPV6 (transient receptor potential channel, vanilloid subfamily)/olfaction, osmosensation, mechanosensation, chemosensation/ankyrin repeat
alh-2	Yeast Ald5 mitochondrial aldehyde dehydrogenase/uncharacterized gene/aldehyde dehydrogenase domain
F08B4.4	Nematode-specific/uncharacterized/novel
C49C8.2	Nematode-specific/uncharacterized/novel
C34C12.4	Human uncharacterized gene/uncharacterized/novel